SSZ-53 and SSZ-59: Two Novel Extra-Large Pore Zeolites

Allen Burton,* Saleh Elomari,* Cong-Yan Chen, Ronald C. Medrud, Ignatius Y. Chan, Lucy M. Bull, Charles Kibby, Thomas V. Harris, Stacey I. Zones, and E. Steven Vittoratos[a]

Abstract: The syntheses, structure solutions, and physicochemical and catalytic characterizations of the novel zeolites SSZ-53 and SSZ-59 are described. SSZ-53 and SSZ-59 were synthesized under hydrothermal conditions with the [1-(4-fluorophenyl)cyclopentylmethyl]trimethyl ammonium cation and 1-[1-(4-chlorophenyl)cyclopentylmethyl]-1-methyl azocanium cation, respectively, as structure-directing agents. The framework topology of SSZ-53 was solved with the FOCUS method, and the structure of SSZ-59 was determined by model building. Rietveld refinement of synchrotron X-ray powder diffraction data confirms each proposed model. SSZ-53 and SSZ-59 each possess a one-dimensional channel system delimited by 14-membered rings. Results from transmission electron microscopy, electron diffraction, catalytic experiments (spaciousness index and constraint index tests), and argon and hydrocarbon adsorption experiments are consistent with the proposed structures.

Keywords: SSZ-53 · SSZ-59 · structure elucidation · synthetic methods · zeolites

Introduction

Because of molecular size restrictions imposed by currently known zeolites, there is continued interest in the synthesis of extra-large pore materials that may be used for hydrocracking large molecules present in heavy oil fractions as well as for facilitating the reactions of molecules involved in the production of fine chemicals. While mesoporous aluminosilicates such as MCM-41 and MCM-48 have pore dimensions between 20 and 200 Å,[1] they lack aluminum in well-defined tetrahedral sites and are closer to amorphous materials than to zeolites in their catalytic behavior.[2,3]

To date several extra-large pore (i.e., a pore delimited by rings with more than 12 tetrahedral (T) atoms), phosphate-based molecular sieves have been prepared. Notable examples include ALPO-8 (**AET**, 14-membered ring or 14-ring, 7.9×8.7 Å),[4] VPI-5 (**VFI**, 18-ring, 12.1 Å),[5] cloverite (**CLO**, 20-ring, 13.2×4.0 Å),[6] JDF-20 (20-ring), the zinco-phosphate ND-1 (24-ring, 10.5 Å),[7] and the gallium phosphate NTHU-1 (24-ring, 10.4 Å).[8] Zhou et al. have also prepared a germanate (FDU-4)[9] that possesses 24-ring pores (9.7 Å). Although a few of the phosphates have pore windows with 20 or more T atoms, their highly puckered apertures are actually more narrow than others observed in structures with fewer T atoms in their pore windows.

Relatively few extra-large pore silicates have been reported. Kongshaug et al. synthesized the beryllosilicate OSB-1 (Si/Be = 2, 7.3×5.4 Å) with 14-ring pores,[10] and Strohmaier and Vaughan recently reported the structure of a gallosilicate (Si/Ga ≅ 3) with 18-ring pores (ECR-34,[11] 10.5 Å). Despite their large pore dimensions, the chemical properties or thermal instabilities of these molecular sieves limit their use as potential catalysts. It therefore remains a challenge to zeolite chemists to prepare extra-large pore materials that may compete as useful catalysts.

Recent reports have increased optimism in the possibility of synthesizing extra-large pore zeolites that possess both thermal stability and favorable Brønsted acidity. UTD-1[12] [as well as its ordered polymorph UTD-1F[13] (**DON**, 7.4×9.5 Å)] and CIT-5 (**CFI**, 7.2×7.5 Å)[14] possess one-dimensional channels delimited by 14-ring pores. Although CIT-5 has 14-ring channels, its pore dimensions are approximately the same as those of 12-ring windows found in the three-dimensional channel systems of zeolite Y (**FAU**, 7.5 Å) and zeolite beta (**BEA***, 7.1×7.3 Å). Although quaternary ammonium compounds are conventionally used for the synthesis of high-silica zeolites,[15] UTD-1 requires the expensive

(pentamethyl)cyclopentadienyl cobalticinium complex in its synthesis,[16] and its cost is therefore prohibitive in most potential commercial applications. Here we report the discovery of two novel extra-large pore zeolites, SSZ-53 and SSZ-59, for which quaternary ammonium compounds were used as structure-directing agents. The syntheses, structure solutions, and physicochemical and catalytic characterizations of these two new zeolites are discussed in detail.

Results and Discussion

Preliminary characterization by powder X-ray diffraction and scanning electron microscopy (SEM): Figure 1 shows the powder XRD ($Cu_{K\alpha}$) patterns of the as-made and calcined forms of B-SSZ-53 and B-SSZ-59 (see Experimental
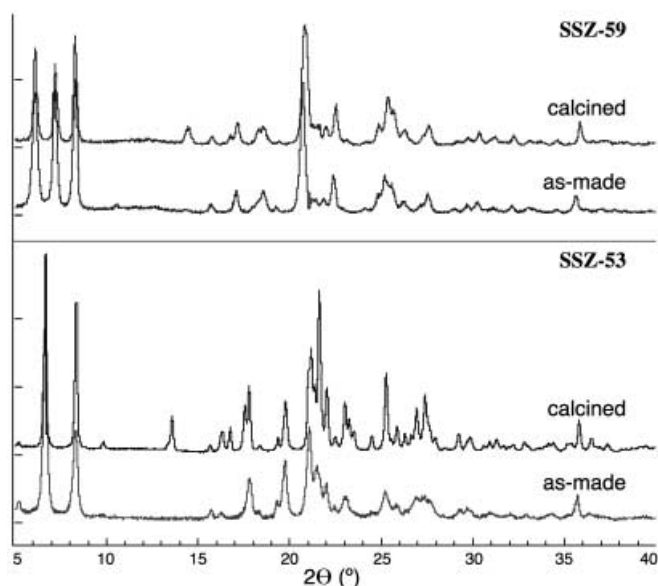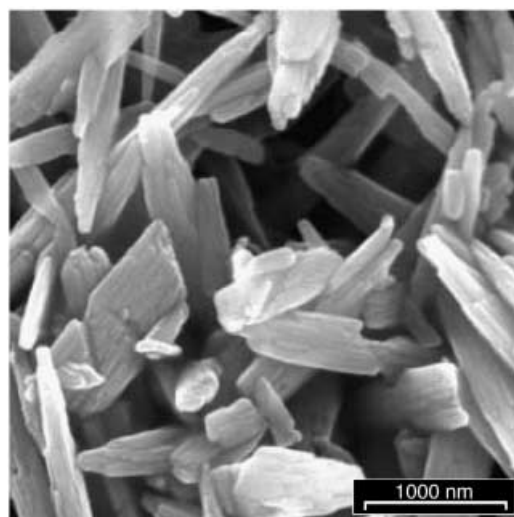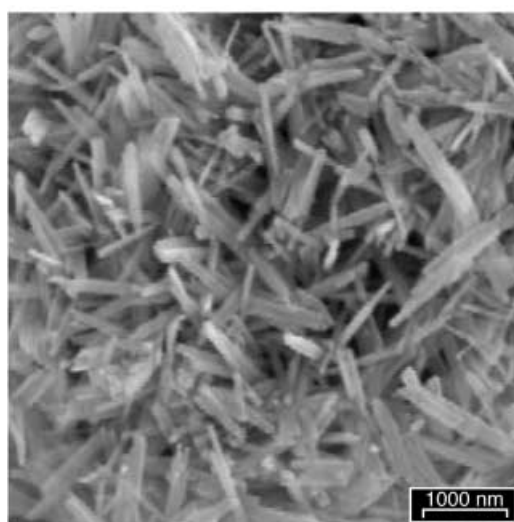

Figure 1. Powder X-ray diffraction patterns of as-made and calcined forms of SSZ-53 and SSZ-59.

a. SSZ-53

b. SSZ-59

Figure 2. SEM micrographs of SSZ-53 (a) and SSZ-59 (b).

Section). The diffraction patterns indicate that both materials are unique zeolite phases and that they remain crystalline after calcination up to 595°C. SEM micrographs of SSZ-53 (Figure 2a) show the basic morphology of the crystals to be in the form of thin laths, approximately 1–2 microns in length, 0.25 microns in width, and 0.05–0.1 microns in thickness. The SEM micrographs of SSZ-59 (Figure 2b) show agglomerates of needle-like crystals about 1 micron in length and less than 0.2 microns in thickness.

Adsorption in SSZ-53 and SSZ-59: The calcined forms of B-SSZ-53 and B-SSZ-59 have micropore volumes of 0.13 and 0.14 mL g^{-1}, respectively, as determined from argon adsorption by the conventional t-plot method. The DFT model for SSZ-53 indicates that about 90% of the microporosity has a diameter centered about 8.3 Å with the remaining porosity having a pore diameter of 5.3 Å. On the other hand, the DFT analysis for SSZ-59 indicates that all the microporosity

has a pore diameter (actually twice the radius of curvature on the pore wall) centered about 8.0 Å. Figures 1Sa and 1Sb in the Supporting Information show the DFT analyses of the pore dimensions.

SSZ-53 and SSZ-59 were also studied with vapor phase hydrocarbon adsorption and compared with zeolites that possess channel systems delimited by medium (10-ring), large (12-ring), and extra-large (≥14-ring) pores:

1) 14-Ring channel zeolites: UTD-1 and CIT-5.
2) Three-dimensional 12-ring channel zeolite:NaY (**FAU**, 7.5×7.5 Å pore window with 13.0 Å supercage).
3) One-dimensional 12-ring channel zeolite: SSZ-55 (**ATS**, 6.5×7.2 Å).[17]
4) Multidimensional pore zeolite with an intersecting 12/12/10-ring channel system: SSZ-33 (similar to **CON**, 12-ring pores of 6.4×7.0 Å and 5.9×7.0 Å, 10-ring windows of 5.1×4.5 Å).[18]
5) Three-dimensional 10-ring channel zeolite: ZSM-5 (**MFI**, 5.5×5.1 Å and 5.6×5.3 Å).

Table 1. Hydrocarbon adsorption capacities of SSZ-53, SSZ-59, and other zeolites for adsorbates of varying dimensions.

Adsorbate	Kinetic diameter [Å]	Adsorption capacity [mL g⁻¹]							
		SSZ-53	SSZ-59	UTD-1(DON)	CIT-5(CFI)	NaY(FAU)	SSZ-55(ATS)	SSZ-33(CON)	ZSM-5(MFI)
argon	3.4	0.13	0.14	0.14	0.11	0.30	0.20	0.22	0.16
n-hexane	4.4	0.13	0.16	0.12	0.09	0.28	0.16	0.20	0.17
cyclohexane	6.0	0.10	0.13	0.11	0.09	0.25	0.13	0.20	0.15
2,2-dimethyl-butane	6.2	0.12	0.12	0.12	0.09	0.25	0.14	0.20	0.15
1,3,5-triisopropyl-benzene	8.5	0.13	0.11	0.11	0.04	0.18	0.03	0.04	0.02

The results from hydrocarbon adsorption experiments of these zeolites are shown in Table 1. Note that the UTD-1, SSZ-53, and SSZ-59 adsorption capacities for the bulky 1,3,5-triisopropylbenzene (1,3,5-TIPB) are nearly equivalent. Also note that their 1,3,5-TIPB adsorption capacities are nearly equivalent to their respective argon, n-hexane, cyclohexane, or 2,2-dimethylbutane adsorption capacities. These data demonstrate that much of the micropore volume available to these smaller adsorbate molecules is also accessible by 1,3,5-TIPB in these zeolites.

The pore dimensions in CIT-5 (7.2 × 7.5 Å) and NaY (~7.5 Å) represent an approximate upper "barrier" to the diffusion of the TIPB molecule. The 1,3,5-TIPB adsorption capacity of CIT-5 is less than half the capacity of the smaller absorbates. The CIT-5 pore dimensions are evidently not large enough to accommodate an equal volume of the bulkier molecule. In the case of NaY, although the 1,3,5-TIPB capacity in the 12-ring zeolite is about 30% lower than the capacities for the smaller adsorbates, it is nonetheless a relatively large quantity. The lower capacity suggests that, in contrast to the smaller molecules, the 1,3,5-TIPB molecule must reside only within the large supercages of NaY and not within the pore windows. The 1,3,5-TIPB capacities of the one-dimensional 12-ring zeolite SSZ-55 and the 12/12/10-ring zeolite SSZ-33 are insignificant compared to their respective hexane capacities.[19]

From the adsorption data, we suspected SSZ-53 and SSZ-59 were extra-large pore zeolites with one-dimensional 14-ring channel systems before the crystal structures of the zeolites were determined.[20]

Crystallographic structure analysis

SSZ-53 unit cell determination: The fitted 2θ peak positions of synchrotron X-ray diffraction data for a calcined sample of SSZ-53 (Figure 3) were used as input to the powder diffraction pattern indexing program TREOR99.[21] The program produced a monoclinic cell: $a = 5.013$, $b = 21.165$, $c = 17.056$ Å, $\beta = 98.3°$ ($M_{20} = 25$[22] and $F_{20} = 84$).[23] Table 1 in the Supporting Information lists the hkl assignments of the peaks. The systematic absences narrow the likely space groups to $P2_1$ or $P2_1/m$.

SSZ-53 structure solution: The framework topology of SSZ-53 was determined with the FOCUS Fourier recycling method. Peak intensities were extracted from the powder pattern by means of the Le Bail method in GSAS.[24] Peaks between 4 and 60° 2θ (resolution of 1.2 Å) were included in the structure solution. Figure 4 shows a projection along the

a axis of the predominant framework structure (without oxygen atoms) obtained from the FOCUS topology search. There was excellent qualitative agreement between the experimental and calculated XRD patterns of this model. Consistent with our conjectures from the adsorption data, this structure possesses one-dimensional 14-ring channels. The DLS R value of this framework is 0.4%, indicating a chemically sensible structure. The highest topological space group symmetry is $C2/c$ with cell dimensions $a = 5.019$, $b = 33.744$, $c = 21.165$ Å, $\beta = 90.5°$. This topology has 8 T atoms (T = te-
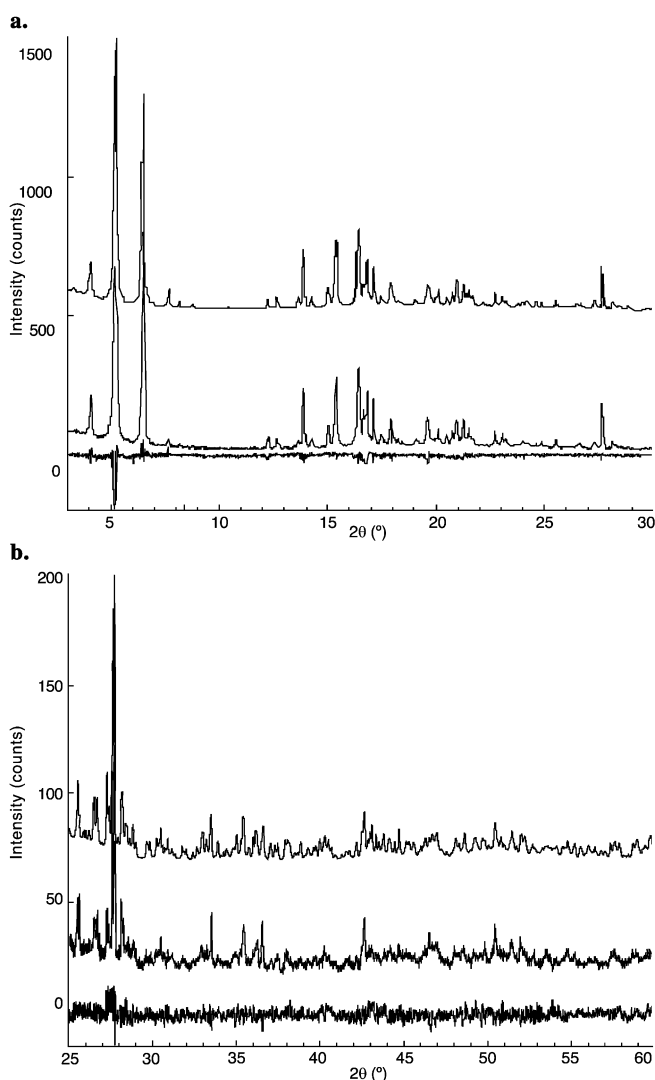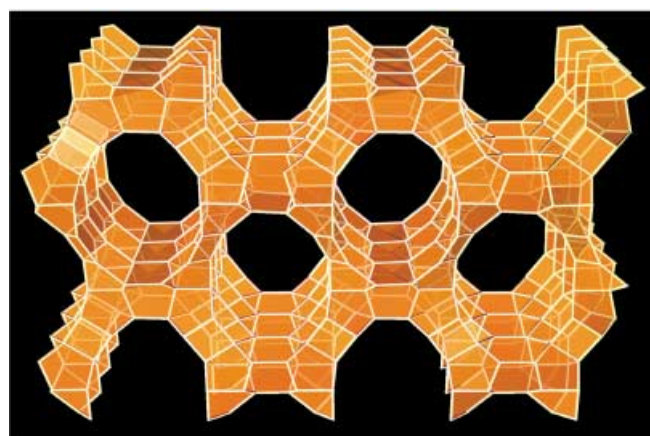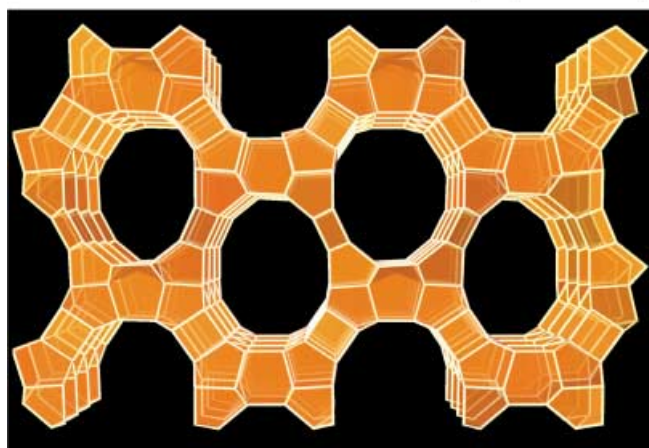

Figure 3. Simulated (top), experimental (middle), and difference (bottom) profiles for the synchrotron X-ray diffraction pattern of SSZ-53 ($\lambda = 1.19963$ Å).

3D Models Created by Kelly and Scott Harvey

Figure 4. Projection of the SSZ-53 framework topology along the *a* axis. Oxygen atoms have been omitted for clarity.

Figure 5. a) TEM micrograph and b) corresponding Fourier transform of SSZ-59 along the [010] zone axis of the monoclinic cell.

trahedral) and 17 oxygen atoms per asymmetric unit, 17.8 T atoms per 1000 Å^3, and a calculated density of 1.79 g cm^{-3}.

TEM analysis of SSZ-59: We were unable to index the powder X-ray diffraction patterns of the as-made and calcined forms of SSZ-59. However, electron diffraction and TEM data collected on SSZ-59 are consistent with the model we ultimately selected for the structure of SSZ-59 (vide infra). Figure 5a shows a TEM image of SSZ-59 and its corresponding Fourier transform (Figure 5b) along the [010] zone axis; these are consistent with a monoclinic cell that possesses dimensions $a = 24.9$, $c = 14.7$ Å, and $\beta = 104°$. The transform image has *d*-spacings that correspond to the 001 (14.3 Å), 200 (12.1 Å), 20$\bar{1}$ (10.5 Å), and 201 (8.3 Å) reflections. In the TEM image it is apparent that, in projection, the centers of the micropores are separated by approximately 12.5 Å along the *a* axis and 14.7 Å along the *c* axis. The angle between the pore centers is about 104°.

SSZ-59 structure solution: The adsorption data for SSZ-59 suggests this structure also possesses one-dimensional 14-ring channels. However, we were initially unable to obtain a satisfactory indexing of the synchrotron XRD pattern. Examination of the SSZ-59 synchrotron diffraction data indicates the presence of a strong reflection at about 16.1° 2θ

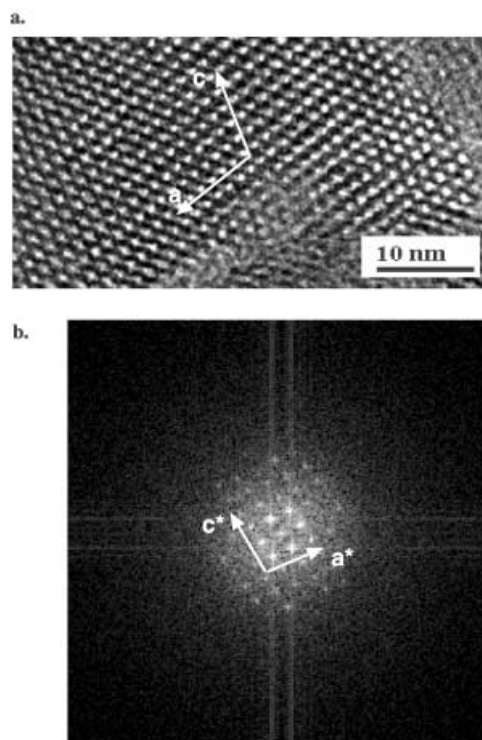(*d*-spacing of 2.51 Å). In many other zeolite structures (SSZ-53, for example), strong peaks with this approximate *d*-spacing often correspond to the second-order reflection of a 5 Å repeat distance.

The "σ-expansion" is a common theme relating different zeolite structures.[25] A σ-expansion may occur by the insertion of 4-ring units between adjoining ring structures. The **TON** (10-ring) and **SFE** (12-ring) frameworks[26], as well as the series of disordered zeolites that includes ZSM-48[27] (10MR)/SSZ-31[28] (12-ring)/UTD-1 (14-ring) (Figure 6), illustrate how frameworks may be derived by σ-expansions between the [5^4.6^1] or "butterfly" units of known structures. We then hypothesized the SSZ-59 framework may be derived either from a σ-expansion of a known zeolite framework or from different symmetry operations performed on layers present in other 14-ring zeolites. We therefore considered zeolite topologies that possess 1) one-dimensional channels and 2) unit cells with 5 Å repeats along their pore axes: **CAN**, **TON**, **MTT**, and **MTW**. Since the σ-expansion of **CAN** requires juxtaposition of 4-ring units in projection along the pore axis (a highly unusual feature in zeolites), we did not pursue this model.

Figure 7 shows 14-ring structures derived from σ-expansions of the **TON**, **MTT**, and **MTW** frameworks. Also shown are 14-ring models derived by relating MTW14MR layers by mirror planes perpendicular to the two types of 4-ring units rather than by relating the layers by translations (MTW14MR b and MTW14MR c).[29] After the appropriate space group of each topology was determined, the frameworks were optimized by energy minimizations (by using the Burchart universal force field) of the atomic coordinates
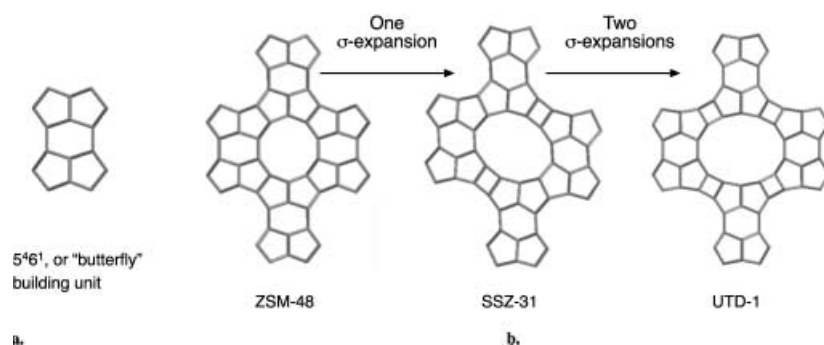
Figure 6. a) "Butterfly" unit of ZSM-48, SSZ-31, and UTD-1. b) Insertion of a single pair of 4-member rings (a σ-expansion) between the butterfly ($5^4 6^1$) units of ZSM-48 yields an SSZ-31 polymorph, and insertion of two pairs of 4-ring units yields a UTD-1 polymorph.
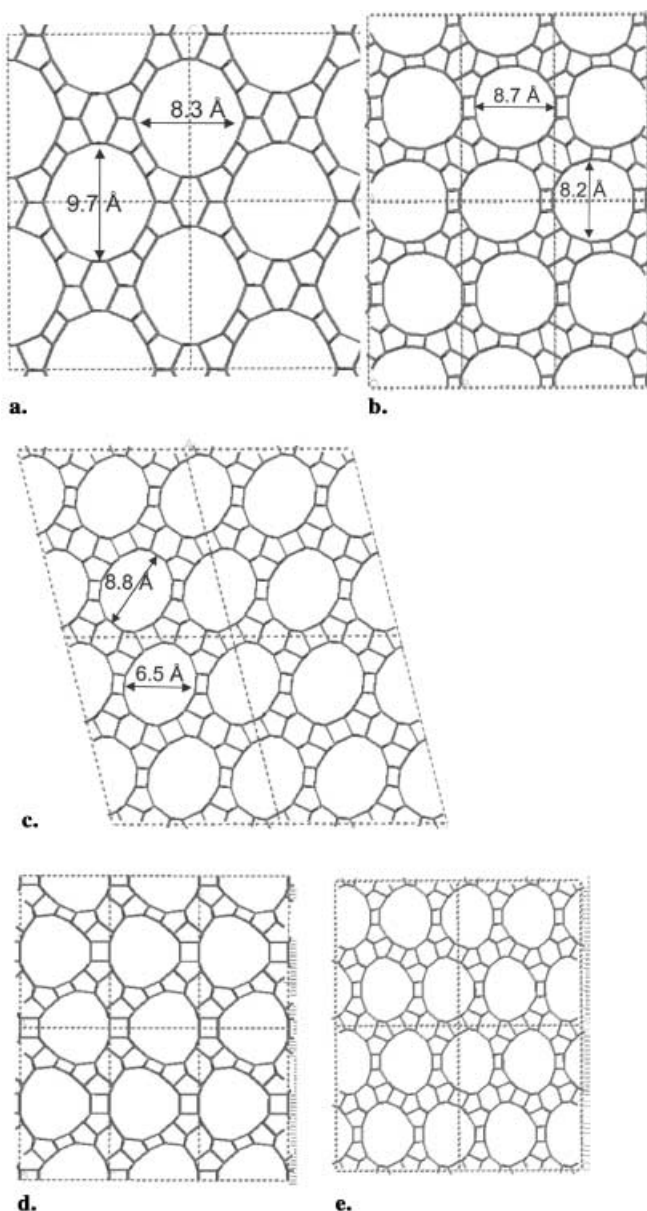
and the unit cell parameters. The coordinates, unit cell parameters, and space group of each framework are given in Tables 2Sa–g in the Supporting Information. The simulated powder XRD patterns of the models and the experimental pattern of SSZ-59 are compared in Figure 8.

Note the close similarity of the SSZ-59 pattern with that of the MTW14MR model. The dimensions between the pore centers of the model are also consistent with the electron diffraction and TEM data. We therefore chose this model, produced by σ-expansion of **MTW**, as the starting point for the Rietveld refinement of the SSZ-59 synchrotron data. Figure 9 shows a projection of the proposed model. This structure has topological space group symmetry $C2/m$ with $a = 24.9$, $b = 5.04$, $c = 14.7$ Å, and $\beta = 104°$. This framework topology has 8 T atoms and 16 O atoms per asymmetric unit, 17.9 T atoms per 1000 Å^3, and a calculated density of 1.78 g cm^{-3}.
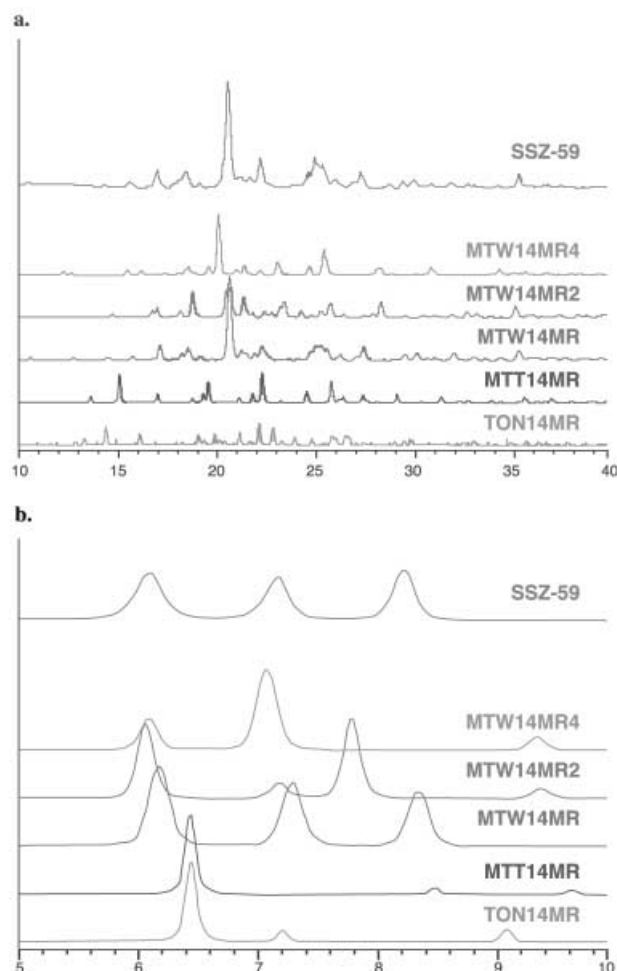

Figure 7. Hypothetical 14-ring zeolites obtained by σ-expansions of a) **TON**, b) **MTT**, and c) **MTW** frameworks. Also shown are 14-ring models derived by relating MTW14MR layers by mirror planes perpendicular to each of the two types of 4-ring units rather than by translations (d and e).

Figure 8. Simulated powder X-ray diffraction patterns ($Cu_{K\alpha}$) of hypothetical 14-ring zeolites.
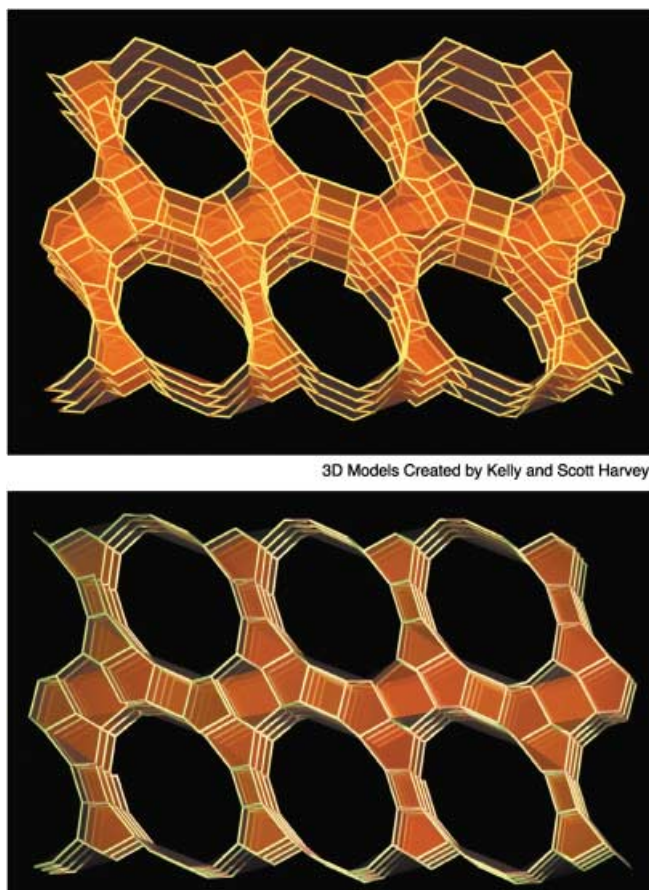
3D Models Created by Kelly and Scott Harvey

Figure 9. Projection of the SSZ-59 framework topology along the *b* axis of the proposed monoclinic cell. Oxygen atoms have been omitted for clarity.

Table 2. Refined atomic parameters of SSZ-53 in space group $C2/c$ (No. 15) ($a = 5.01920(9)$, $b = 33.7437(9)$, $c = 21.1653(6)$ Å, $\beta = 90.485(8)°$).

atom	x	y	z
Si1	0.551(2)	0.6108(2)	0.5041(4)
Si2	0.056(2)	0.5621(2)	0.5206(4)
Si3	0.534(2)	0.6985(2)	0.9880(5)
Si4	0.457(2)	0.3787(2)	0.6453(4)
Si5	0.947(2)	0.4892(3)	0.6025(4)
Si6	0.457(2)	0.4670(2)	0.6784(3)
Si7	0.955(2)	0.3322(2)	0.6790(3)
Si8	0.037(2)	0.2763(3)	0.5707(4)
O1	0.332(2)	0.2892(5)	0.5454(6)
O2	0.484(3)	0.3850(5)	0.5710(3)
O3	0.492(3)	0.3460(2)	0.4656(6)
O4	0.5	0.5176(4)	0.25
O5	0.996(3)	0.5332(3)	0.5782(7)
O6	0.346(2)	0.5801(4)	0.5308(6)
O7	0.843(2)	0.5966(3)	0.5214(7)
O8	0.162(2)	0.4768(4)	0.6548(5)
O9	0.659(3)	0.4877(4)	0.6326(5)
O10	0	0.6811(5)	0.25
O11	0.990(3)	0.2931(3)	0.6378(4)
O12	0.658(2)	0.3470(4)	0.6705(6)
O13	0.161(2)	0.3648(4)	0.6605(7)
O14	0.509(4)	0.7290(3)	0.5698(6)
O15	0.957(3)	0.4610(5)	0.5434(5)
O16	0.488(3)	0.4203(2)	0.8220(7)
O17	0.168(2)	0.2948(5)	0.9834(6)

space group $C2/m$, the highest topological symmetry of the proposed structure. However, the peak intensities were not modeled well using this space group. In addition, the proposed unit cell could not account for all of the peaks observed in the mid-angle range of the diffraction pattern. Furthermore, the bond lengths and angles were well outside the normal range of values although restraints were imposed. Figure 2S in the Supporting Information demonstrates the poor agreement between the experimental and calculated profiles in space group $C2/m$.

We therefore decided to lower the symmetry to $P\bar{1}$. This space group could account for all observed peaks, the peak shapes and peak intensities were adequately modelled, and the bond lengths and angles were within a reasonable range of values. Figure 10 shows the observed, calculated, and difference profiles for the synchrotron X-ray diffraction data of SSZ-59. Table 5S in the Supporting Information summarizes the final details of the refinement. The R_{wp} and R_p agreement values were 5.51% and 4.91%, respectively. Table 3 shows the refined atomic coordinates of SSZ-59. Tables 6Sa and 6Sb in the Supporting Information give the final bond lengths and angles for the refined structure. It should be noted that these values are affected by distance restraints used throughout the refinement. However, the refinement does show that good qualitative and quantitative agreement is obtained for a proposed topological structure that has reasonable bond lengths and angles.

Rietveld refinement of SSZ-53: The starting model for the Rietveld refinement of SSZ-53 was obtained from the FOCUS structure solution. A six-term Chebyshev polynomial was used to model the background. Peak shapes were modeled with the pseudo-Voigt function of Howard[30] and Thompson et.al.[22] Atoms of identical element type were constrained to have the same isotropic thermal displacement parameters. Soft distance restraints were placed on the bonds between the silicon and oxygen atoms (Si–O ~ 1.60 ± 0.03 Å), the distances between tetrahedral oxygen atoms (O–O ~ 2.61 ± 0.04 Å), and the distances between neighboring T atoms (3.08 ± 0.05 Å).

The refinement converged to R_p and R_{wp} values of 6.69% and 8.75%, respectively. The Si–O distances and tetrahedral angles (see Supporting Information Tables 3Sa and 3Sb) are within a reasonable range of values. Table 4S in the Supporting Information summarizes the final details of the refinement, and Table 2 gives the refined atomic parameters of SSZ-53.

Rietveld refinement of SSZ-59: The starting model for the refinement of SSZ-59 was the 14-ring zeolite formed by the σ-expansion of **MTW**. The background, peak-shape functions, and restraints were the same ones used in the refinement of SSZ-53. The refinement was initially performed in

Structural features of SSZ-53 and SSZ-59: The framework structures of SSZ-53 and SSZ-59 (Figure 4 and 9) are very similar. They both have elliptical 14-ring pores with dimensions (adjusted for the radius of oxygen ≈ 1.35 Å) of approximately 8.5 × 6.5 Å. They also possess the same frame-
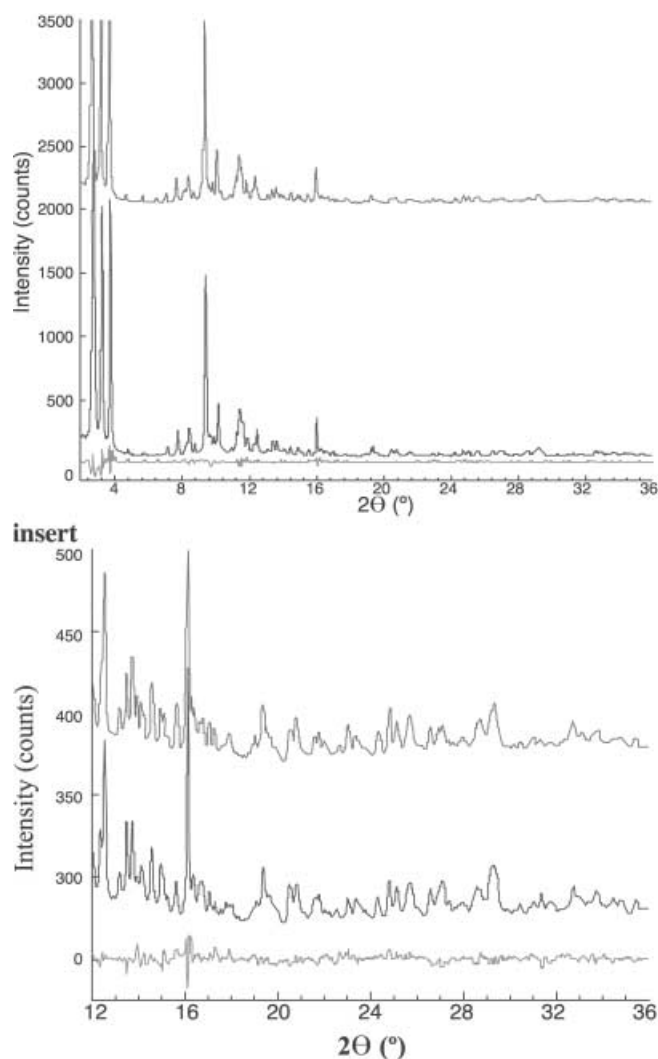
Figure 10. Simulated (top), experimental (middle), and difference (bottom) profiles for the synchrotron X-ray diffraction pattern of SSZ-59 ($\lambda = 0.703867$ Å).

Table 3. Refined atomic parameters of SSZ-59 in space group $P\bar{1}$ ($a = 5.0231(1)$, $b = 12.7351(7)$, $c = 14.7219(8)$ Å, $\alpha = 103.44°$, $\beta = 90.51°$, $\gamma = 100.88°$).

| atom	x	y	z
Si1	0.104(2)	0.0959(8)	0.6362(7)
Si2	0.680(2)	0.4459(8)	0.3118(7)
Si3	0.662(2)	0.2151(7)	0.7202(7)
Si4	0.690(2)	0.2714(7)	0.4214(8)
Si5	0.750(2)	0.4131(8)	0.6226(7)
Si6	0.665(2)	0.3797(8)	0.9041(7)
Si7	0.750(2)	0.4731(8)	0.1124(7)
Si8	0.131(2)	0.1485(8)	0.4432(7)
O1	0.994(4)	0.9703(9)	0.624(1)
O2	0.410(3)	0.119(1)	0.681(1)
O3	0.068(3)	0.832(1)	0.297(1)
O4	0.117(4)	0.134(1)	0.5437(8)
O5	0.984(3)	0.238(1)	0.421(1)
O6	0.553(3)	0.826(1)	0.584(1)
O7	0.673(4)	0.331(1)	0.3368(9)
O8	0.414(3)	0.491(1)	0.344 (1)
O9	0.067(3)	0.464(1)	0.644 (1)
O10	0.681(4)	0.421(1)	0.1999(7)
O11	0.639(4)	0.259(1)	0.8313(8)
O12	0.664(4)	0.314(1)	0.672(1)
O13	0.684(4)	0.366(1)	0.5135(7)
O14	0.694(5)	0.378(1)	0.0146(7)
O15	0.920(3)	0.467 (1)	0.880(1)
O16	0.596(3)	0.570 (1)	0.113(1)
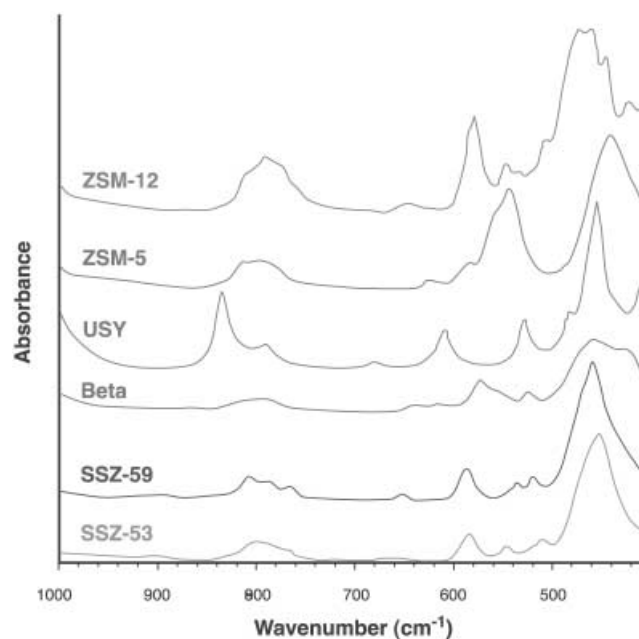
Figure 11. The infrared spectra of the calcined forms of SSZ-53, SSZ-59, and other representative zeolites.

work density. Figure 11 compares the infrared spectra of the calcined forms of SSZ-53 and SSZ-59 with those of other representative zeolites. The overlapping bands are consistent with a pair of silicate structures that have striking similarity in their ring features. However, the differences observed within 600–500 cm^{-1} indicate that the structures are indeed distinct. In fact, the topological structures can be derived from different symmetry operations performed on the same subunit. Figure 12 show the structural relationship between SSZ-53 and SSZ-59. While the layers in SSZ-53 are related by a twofold rotation about an axis within the plane of the figure, the layers in SSZ-59 are related by a twofold rotation about an axis perpendicular to the figure.

The subtle differences between SSZ-53 and SSZ-59 are exemplified in their different pore structures. Figure 13 shows the pore structures of SSZ-53, SSZ-59, and UTD-1. While UTD-1 possesses pores bound by smooth 6-ring ring nets, both SSZ-53 and SSZ-59 have pores with corrugated surfaces. In SSZ-53 these corrugations are centered about the vertices (of the major axis) of the elliptical pore. On the

other hand, in SSZ-59 the corrugations are positioned on the sides (i.e., near the vertices of the minor axis) of the elliptical pore.

DFT analyses of adsorption data yield information about the local radius of curvature on the pore surface. It is for this reason that approximate dimensions obtained from these calculations often show a broad (± 1.5 Å) distribution with maxima at certain characteristic values. In both SSZ-53
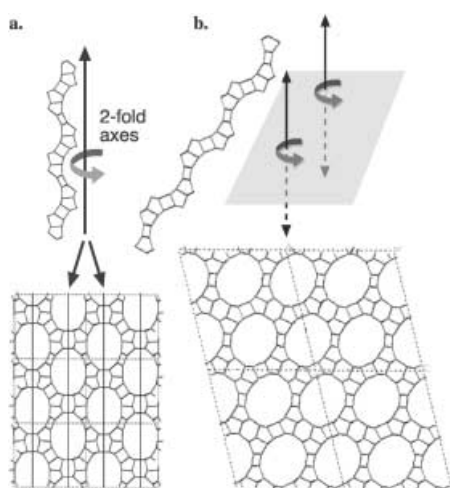
Figure 12. Structural relationship between a) SSZ-53 and b) SSZ-59. The layers in SSZ-53 are related by rotations about twofold axes within the plane of the figure. The layers in SSZ-59 are related by rotations about twofold axes perpendicular to the plane of the figure.
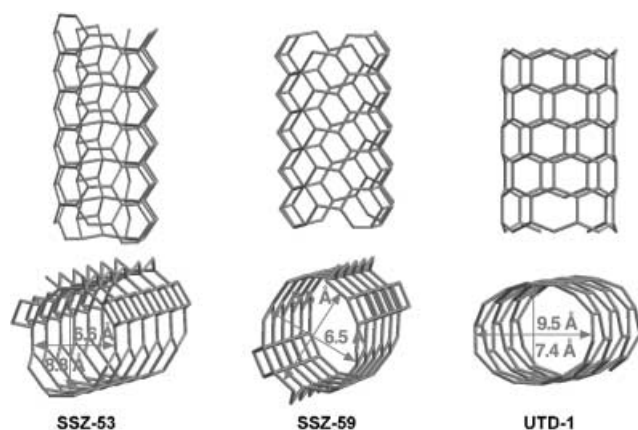
$23.5\,Si:0.6\,B:15.2\,C:1\,N:24.5\,H$. The C:N:H ratio is close to the chemical formula of the SDA:$C_{15}H_{23}NF$ (SDA = structure-directing agent). The T atom/SDA ratio (on a carbon basis) is 24. This is equivalent to $^{4}/_{3}$ SDA molecules per unit cell. TGA measurements are consistent with the results of the chemical analyses.

Chemical analyses of as-made SSZ-59 indicate atomic ratios of $32.4\,Si:0.7\,B:18.5\,C:1.0\,N:28.0\,H$. The atomic ratios of the organic component are in excellent agreement with the chemical formula of the SDA:$C_{18}NH_{28}$. The T atom/SDA ratio (on a carbon basis) is 32, equivalent to 1 SDA per unit cell. TGA measurements of the organic loss are in close agreement with the results of the chemical analyses. Furthermore, ^{13}C CP MAS NMR experiments on the as-made forms of SSZ-53 and SSZ-59 indicate the organic SDAs remain intact within the void space of each zeolite. Figure 14 shows the ^{13}C CP NMR spectra and the assignments of the carbon atoms.
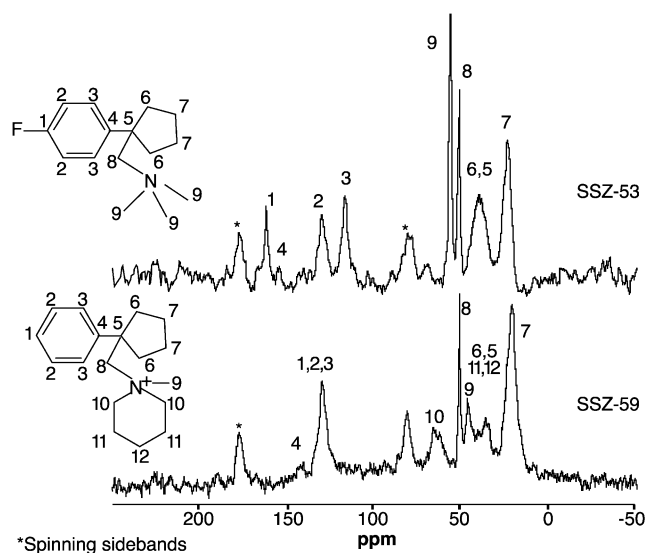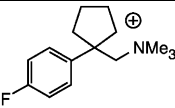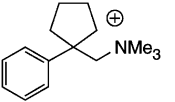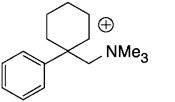

Figure 13. Comparison of the pore structures in SSZ-53, SSZ-59, and UTD-1.
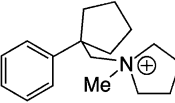
Figure 14. ^{13}C CP MAS NMR spectra and peak assignments of the as-made forms of (top) SSZ-53 and (bottom) SSZ-59.

and SSZ-59, maxima are observed near 8 Å (Supporting Information Figures 1Sa and 1Sb). This is not a surprising result given the pore dimensions of the crystallographic structure. However, in SSZ-53 about 10% of the microporosity is centered about 5.3 Å. This is a reproducible result observed in different preparations of SSZ-53. Why is this observed in SSZ-53 and not in SSZ-59? A possible explanation may be found in the positions of the pore corrugations in each structure. Adsorption simulations show that (for SSZ-53 and SSZ-59) the centers of these corrugations provide ideal adsorption sites for small molecules like helium or argon. In SSZ-59 the corrugations are positioned on the "sides" of the elliptical pores, where the curvature is a minimum; however, in SSZ-53, these corrugations are located near the pore vertices, where the curvature is a maximum. This may explain why a small fraction of the microporosity in SSZ-53 is associated with a dimension of 5.3 Å.

Host–guest interactions: Chemical analyses of as-made B-SSZ-53 indicate atomic ratios of

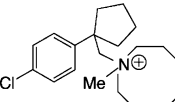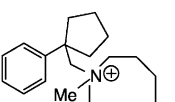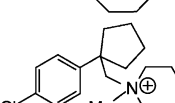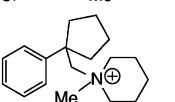In an attempt to rationalize the structure-directing effects, we performed energy minimization calculations (see Experimental Section for details) of each SDA (Table 4) within the very similar frameworks of SSZ-53 and SSZ-59. The stabilization energy of each molecule was determined by calculating the energy difference of the free molecule and the molecule occluded within the zeolite framework. In the case of the SDAs that produce SSZ-59, a super cell of four unit cells in length along the pore direction was created. This allowed sufficient space to accommodate two molecules within each pore of the super cell. Note that this complies with the results of the chemical analysis. Since only two unit cells would force each molecule to adopt the same configuration as its nearest neighbor within the pore, four unit cells were chosen to allow more configurational freedom. In the case of the SDAs that produce SSZ-53, a super cell was created three unit cells in length along the pore direction in order 1) to comply with the results of the chemi-

Table 4. Stabilization energies calculated for each structure-directing agent within the frameworks of SSZ-S3 and SSZ-59. For the SDAs that produce SSZ-53, the supercells were three unit cells in length along the pore axis, while the supercells for the SSZ-59 SDAs were four unit cells in length along the pore axis.

Molecule	$N^{[a]}$	$E_{SSZ-53}^{[b]}$ [KJ per mol SDA]	$E_{SSZ-59}^{[c]}$ [KJ per mol SDA]	$E_{SSZ-53}^{[b]}$ [KJ per mol T atoms]	$E_{SSZ-59}^{[c]}$ [KJ per mol T atoms]
53SDA1	2	−192	−174	−8.0	−7.3
53SDA2	2	−194	−174	−8.1	−7.3
53SDA3	2	−167	−149	−7.0	−6.2
53SDA4	2	−181	−130	−7.5	−5.4
59SDA1	2	−170	−171	−5.3	−5.3
59SDA2	2	−175	−186	−5.5	−5.8
59SDA3	2	−197	−191	−6.2	−6.0
59SDA4	2	−186	−183	−5.8	−5.7

[a] N = number of SDA molecules per supercell. [b] E_{SSZ-53} = Stabilization energy in SSZ-53. [c] E_{SSZ-59} = Stabilization energy in SSZ-59.

cal pores. The long dimensions of the SDA molecules are positioned perpendicular to the pore axis in all cases. Figure 15b and d show views perpendicular to the pore axes. The neighboring molecules adopt different orientations in order to enhance the van der Waals interactions between each molecule. Note that these positions also affect the relative locations of the nitrogen atoms. It is doubtful that the negative framework charges are positioned on special T atom sites. However, it is not unreasonable to expect the charges may alternate in an up/down fashion that reflects the sinusoidal arrangement of the nitrogen atoms along the pore axis.

Since SSZ-53 and SSZ-59 have remarkably similar pore structures, it is not surprising that most of the SDA molecules show similar stabilization energies within their respective frameworks. Although the stabilization energies for the SSZ-53 SDAs are slightly better in SSZ-53 than in SSZ-59, the differences are not significant enough to differentiate the structure-directing effects of each molecule. Likewise, the SSZ-59 SDAs show negligible differences in energy between the two frameworks. One interesting exception is 53SDA4, which shows a 50 kJ per mol T atom difference in the stabilization energies within the two frameworks. This molecule possesses two rigid cyclopentyl rings. In its optimized configuration within each framework, one of the cyclopentyl rings points directly into the upper (or lower) region of the elliptical pore. As mentioned above, the pore corrugations in SSZ-53 are located in the upper region of the pores, while the pore corrugations in SSZ-59 are positioned on the sides of the pores. The small volume of space afforded by the corrugation in SSZ-53 allows a more energetically stable interaction between the pore wall and the cyclopentyl ring.

Catalytic characterization: Samples of Al–SSZ-53 and Al–SSZ-59 were characterized by the constraint index (CI) test. The CI is widely used to characterize the effective pore size of acidic zeolites. The CI is based upon a comparison of the cracking rates of n-hexane and 3-methylpentane with an equimolar mixture of these two hydrocarbons as feed.[32,33] The Al–SSZ-53 and Al–SSZ-59 samples studied here have

cal analysis and 2) to again place two molecules within each pore. At least 20 different configurations of the SDAs were sampled for each framework by placing two molecules in random locations within the void space of each pore.

Table 4 gives the minimum energies found for each molecule/framework pair. All of the SDA molecules have highly favorable stabilization energies within the frameworks of both SSZ-53 and SSZ-59. Indeed these energies are even lower than those found in other zeolite/SDA systems;[31] however, it must also be borne in mind that the SDAs for SSZ-53 and SSZ-59 are slightly larger than those typically examined in zeolite host–guest interactions. These molecules have 15–20 C atoms and the effects of van der Waals interactions with zeolite framework are therefore expected to be more pronounced.

Figure 15a and c show space-filling models of the optimized configuration of 53SDA4 within the frameworks of SSZ-53 and SSZ-59. The views down the pore axes illustrate the similarity in the shapes of the molecules and the ellipti-
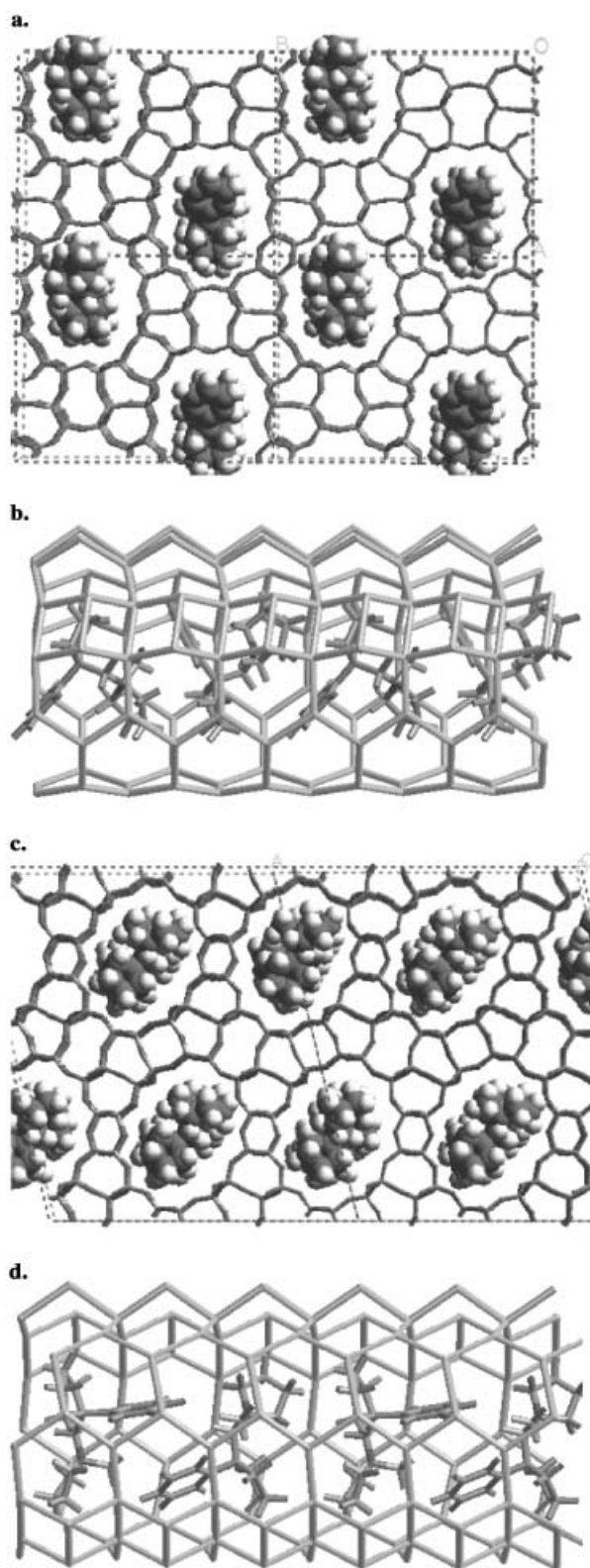
Figure 15. View of the energy-optimized configuration of 1-methyl-1-(1-phenylcyclopentylmethyl)pyrrolidinium in a) SSZ-53 (view down pore axis), b) SSZ-53 (view perpendicular to pore axis), c) SSZ-59 (view down pore axis), d) SSZ-59 (view perpendicular to pore axis). Space-filling models have been used for the organic cation in a) and c) to illustrate the similarity in the shape of the pores and the structure directing agent. Oxygen atoms have been removed in b) and d) for clarity.

CI values of 0.73 and 0.27, respectively, which are typical of 12-ring or larger pore zeolites.

The above Al–SSZ-53 and Al–SSZ-59 materials were also loaded with 0.27 wt % Pd by means of ion exchange with an aqueous solution of $[Pd(NH_3)_4](NO_3)_2$. The resulting Pd/Al–SSZ-53 and Pd/Al–SSZ-59 species were characterized by using the spaciousness index (SI) test. The SI is defined as the yield ratio of iso-butane to *n*-butane in the hydrocracking of a C_{10}-cycloalkane, such as *n*-butylcyclohexane, over bifunctional zeolites or other molecular sieve materials.[34–36] The ratio increases with increasing pore size and is proven to be a useful tool for characterizing the shape-selective properties of molecular sieve materials. Based on our results, SSZ-53 and SSZ-59 have an SI of 20 and 19, respectively. In Figure 16, the SI values of SSZ-53 and SSZ-59 are
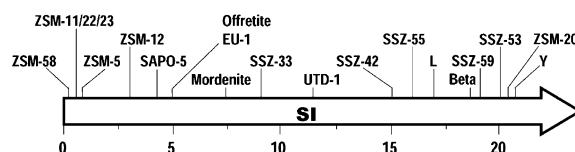

Figure 16. A comparison of the spaciousness indices (SI) of SSZ-53, SSZ-59, and other representative zeolites.

compared to those reported for other zeolites. According to the above results, the effective void sizes of SSZ-53 and SSZ-59 are smaller than the effective diameter of the largest voids in zeolite Y and ZSM-20, but larger than those of 12-ring zeolites, such as beta and L. The high SI values of SSZ-53 and SSZ-59 provide another piece of experimental evidence that is consistent with the structures determined in this work.

Conclusions

The syntheses, characterizations, and structure solutions of the novel zeolites SSZ-53 and SSZ-59 have been reported. SSZ-53, SSZ-59, UTD-1, and CIT-5 are the only extra-large pore high-silica zeolites reported to date. Unlike UTD-1, which is synthesized in the presence of an organometallic SDA, SSZ-53 and SSZ-59 are prepared by means of quaternary ammonium compounds. Furthermore, SSZ-53 and SSZ-59 have pores that are larger than those present in CIT–5.

The structures of SSZ-53 and SSZ-59 were determined by the FOCUS method and by model building, respectively. Rietveld refinements of synchrotron X-ray powder diffraction data confirm the proposed models. Argon and hydrocarbon adsorption data, as well as spaciousness index (SI) and constraint index (CI) data, also strongly support the proposed 14-ring structures. Results from chemical analyses, TGA measurements, and energy optimizations indicate the host–guest interactions between the organic structure-directing agents and the zeolite framework structures are crucial in preparing these metastable phases.

Experimental Section

Zeolite syntheses: SSZ-53 zeolite was synthesized hydrothermally as a borosilicate or aluminosilicate in the presence of [1-(4-fluorophenyl)cyclopentylmethyl]trimethyl ammonium (**53SDA1**), trimethyl(1-phenylcyclopentylmethyl)ammonium (**53SDA2**), trimethyl(1-phenylcyclohexylmethyl)ammonium (**53SDA3**), or 1-methyl-1-(1-phenylcyclopentylmethyl)-pyrrolidinium (**53SDA4**) cations as structure-directing agents (see Table 4). The detailed syntheses of the zeolite and the structure-directing agents are described elsewhere.[20, 37] SSZ-59 zeolite was synthesized hydrothermally as a borosilicate or aluminosilicate in the presence of 1-[1-(4-chlorophenyl)cyclopentylmethyl]-1-methyl azocanium (**59SDA1**), 1-methyl-1-(1-phenylcyclopentylmethyl)azocanium (**59SDA2**), 1-[1-(4-chlorophenyl)cyclopentylmethyl]-1-methylpiperidinium (**59SDA3**), or 1-methyl-1-(1-phenylcyclopentylmethyl)piperidinium (**59SDA4**) as SDA (Table 4). The detailed syntheses of the zeolite and the structure-directing agents are described elsewhere.[38, 39b]

In a typical synthesis, SSZ-53 or SSZ-59 was prepared by heating a gel mixture composed of a silica source, a sodium borate or aluminum oxide source, sodium hydroxide, the hydroxide form of the SDA, and water. Normally, the molar ratios of the gel components were 0.05 Na_2O:0.10 $(SDA)_2O$:0.022 B_2O_3:41 H_2O:SiO_2. The following procedure is a representative example for preparing the borosilicate version of SSZ-53. In a 23 mL Teflon cup, a solution of [1-(4-fluoro-phenyl)cyclopentylmethyl]trimethyl ammonium hydroxide (3 mmol, 6.33 g of 0.475 molar template solution), NaOH (1.2 mmol, 1.2 g of 1 N aqueous solution), and water (4.45 g) were mixed. Then sodium borate decahydrate ($Na_2B_4O_7 \cdot 10 H_2O$, 0.06 g) was added and stirred until complete dissolution. CAB-O-SIL M-5 (0.9 g, 98% SiO_2 and 2% water) was added to this solution, and the mixture was thoroughly stirred. The resulting gel was capped off, placed in a Parr reactor, and then heated in an oven at 160°C while rotating at 43 rpm. The reaction was monitored by periodically measuring the pH of the gel and checking crystal formation by scanning electron microscopy (SEM). The reaction was typically completed after heating for 18 days (12 days for SSZ-59). The resulting solids were washed with water (1 L) and then allowed to air-dry over night. The reaction typically yielded 0.85 g of SSZ-53. The organic components were removed from the zeolites by calcination to 595°C in an atmosphere of nitrogen containing 2% oxygen.

Analytical methods: Preliminary powder XRD patterns were collected on Siemens D-500 instrument with $Cu_{K\alpha}$ radiation. Scanning electron micrographs (SEM) were collected with a Hitachi S-570. Transmission electron micrographs (TEM) and electron diffraction (ED) patterns were collected with a JEOL 2010 instrument operating at 200 kV. Samples were prepared by dispersing crystallites or microtomed thin sections on a continuous carbon film.

Samples for detailed structural analysis were examined at Beamline X7A at Brookhaven National Laboratory. Synchrotron powder XRD data for SSZ-53 were collected at ambient temperature from 2 to 60° 2θ with a step size of 0.01° 2θ and a wavelength of 1.19963 Å. The X-ray intensity was monitored by means of a scintillation counter. Synchrotron data for SSZ-59 were collected at ambient temperature from 2–36° 2θ with a step size of 0.01° 2θ and a wavelength of 0.70387 Å. The X-ray intensity for the SSZ-59 sample was monitored with a position-sensitive detector (PSD). The X7A samples were prepared in 1.5 mm diameter glass capillaries that were sealed after being evacuated and heated overnight at 350°C. For SSZ-53, the starting model for the Rietveld structure refinement was generated with the FOCUS[39, 40] algorithm. The structure of SSZ-59 was determined by model building. Initial distance least-squares refinements of the starting models were carried out with DLS-76.[41] Energy minimizations of the SDAs within the frameworks were performed with Cerius2 2.1[42] from MSI with the Burchart universal force field.[43] Framework atoms were fixed during the energy minimizations. Contributions from van der Waals interactions and valence bond, angle, and torsion energies were determined with the Burchart universal force field. Coulombic interactions between the cation and the zeolite framework were neglected.

Elemental analyses were performed by Galbraith Laboratories (Knoxville, TN). Thermogravimetric analyses (TGA) of the as-made SSZ-53 and SSZ-59 materials were performed on a Hi-Res TGA 2950 Thermogravimetric Analyzer (from TA Instruments). The samples were heated in air at a rate of 5°C min^{-1} for the data collection.

The pore size and void volumes of the calcined zeolites were probed by physisorption of argon, nitrogen, and a series of hydrocarbon adsorbates. Argon adsorption at −186°C was performed using the Micromeritics ASAP 2010. The samples were first outgassed at 400°C for 16 h prior to argon adsorption. The low-pressure dose was 2.0 cc g^{-1} STP. A maximum of one hour equilibration time per dose was used, and the total run time was 35 h. Deduction of pore dimensions from the adsorption isotherm was performed by means of density functional theory (DFT) as developed by Olivier[44, 45] for graphite slits, by the Saito-Foley adaptation of the Horvathb–Kawazoe thermodynamic formulation,[46] and by the conventional t-plot method.[47] The t-plot analyses were also performed using nitrogen adsorption data collected by the Micromeritics 2400 instrument.

The adsorption capacities of zeolites for vapor phase hydrocarbons were measured at room temperature using a Cahn C-2000 balance. n-Hexane, cyclohexane, 2,2-dimethylbutane, and 1,3,5-triisopropylbenzene were used as "plug gauge" adsorbate molecules with various kinetic diameters. Detailed discussion on hydrocarbon adsorption experiments is reported elsewhere.[48] The constraint index and spaciousness index test reactions were conducted according to the procedures reported elsewhere.[34–38]

Acknowledgement

[1] J. S. Beck, J. C. Vartuli, W. J. Roth, M. E. Leonowicz, C. T. Kresge, K. D. Schmitt, C. T. W. Chu, D. H. Olson, E. W. Sheppard, S. B. McCullen, J. B. Higgins, J. L. Schlenker, *J. Am. Chem. Soc.* **1992**, *114*, 10834–10843.

[2] C. Y. Chen, H. X. Li, M. E. Davis, *Microporous Mater.* **1993**, *2*, 17–26.

[3] A. Corma, *Chem. Rev.* **1995**, *95*, 559–614.

[4] J. W. Richardson, Jr., E. T. C. Vogt, *Zeolites* **1992**, *12*, 13–19.

[5] M. E. Davis, C. Saldarriaga, C. Montes, J. Garces, C. Crowder, *Nature* **1988**, *331*, 698–699.

[6] M. Estermann, L. B. McCusker, C. Baerlocher, A. Merrouche, H. Kessler, *Nature* **1991**, *352*, 320–323.

[7] G. Yang, S. C. Sevov, *J. Am. Chem. Soc.* **1999**, *121*, 8389–8390.

[8] C. Lin, S. Wang, K. Lii, *J. Am. Chem. Soc.* **2001**, *123*, 4649–4650.

[9] Y. Zhou, H. Zhu, Z. Chen, M. Chen, Y. Xu, H. Zhang, D. Zhao, *Angew. Chem.* **2001**, *113*, 2224–2226; *Angew. Chem. Int. Ed.* **2001**, *40*, 2166–2168.

[10] K. O. Kongshaug, H. Fjellvag, K. P. Lillerud, T. E. Gier, G. D. Stucky, A. K. Cheetham, in http://www.iza-structure.org/databases/

[11] K. G. Strohmaier, D. E. W. Vaughn, 2nd FEZA Conference, *Impact of Zeolites and other Porous Materials on the New Technologies at the Beginning of the New Millenium* **2002**, RRR033.

[12] R. F. Lobo, M. Tsapatsis, C. C. Freyhardt, S. Khodabandeh, P. Wagner, C. Y. Chen, K. J. Balkus, S. I. Zones, M. E. Davis, *J. Am. Chem. Soc.* **1997**, *119*, 8474–8484.

[13] T. Wessels, C. Baerlocher, L. B. McCusker, E. J. Creyghton, *J. Am. Chem. Soc.* **1999**, *121*, 6242–6247.

[14] P. Wagner, M. Yoshikawa, M. Lovallo, K. Tsuji, M. Tsapatsis, M. E. Davis, *Chem. Commun.* **1998**, 7139–7147.

[15] R. F. Lobo, S. I. Zones, M. E. Davis, *J. Inclusion Phenom. Mol. Recognit. Chem.* **1995**, *21*, 47–78.

[16] K. J. Balkus, A. G. Gabrielov, US Patent 5489424, **1996**.

[17] M. G. Wu, M. W. Deem, S. Elomari, R. C. Medrud, S. I. Zones, T. Maesen, C. Kibby, C. Y. Chen, I. Y. Chan, *J. Phys. Chem. B* **2002**, *106*, 264–270.

[18] R. F. Lobo, M. E. Davis, *J. Am. Chem. Soc.* **1995**, *117*, 3766–3779.

[19] C. Y. Chen, S. I. Zones, "Investigation of Hydrocarbon Adsorption on Large and Extra-Large Pore Zeolites," in "Zeolites and Mesoporous Materials at the Dawn of the 21st Century," Proceedings of the 13th International Zeolite Conference, Montpellier, France, 8–13 July, **2001**; C. Y. Chen, S. I. Zones, *Stud. Surf. Sci. Catal.* **2001**, *135*, 222.

[20] "Synthesis of Novel Zeolites SSZ-53 and SSZ-55 Using Novel Organic Templating Agents Derived from Nitriles": S. Elomari, S. I. Zones, *Stud. Sur. Sci. Catal.* **2001**, *135*, 479.

[21] P. E. Werner, L. Eriksson, M. Westdahl, *J. Appl. Crystallogr.* **1985**, *18*, 367–370.

[22] P. M. de Wolff, *J. Appl. Crystallogr.* **1968**, *1*, 108–113.

[23] G. L. Smith, R. L. Snyder, *J. Appl. Crystallogr.* 1**979**, *12*, 60–65.

[24] A. C. Larson, R. B. von Dreele, *General Structure Analysis System GSAS*, Los Alamos National Laboratory, Los Alamos, NM, **1994**.

[25] R. M. Barrer, *Zeolites and Clay Minerals as Sorbents and Molecular Sieves* **1978**, p. 63.

[26] P. Wagner, O. Terasaki, S. Ritsch, J. G. Nery, S. I. Zones, M. E. Davis, K. Hiraga, *J. Phys. Chem. B* **1999**, *103*, 8245–8250.

[27] J. L. Schlenker, W. J. Rohrbaugh, P. Chu, E. W. Valyocsik, G. T. Kokotailo, *Zeolites* **1985**, *5*, 355–358.

[28] R. F. Lobo, M. Tsapatsis, C. C. Freyhardt, I. Chan, C. Y. Chen, S. I. Zones, M. E. Davis, *J. Am. Chem. Soc.* **1997**, *119*, 3732–3744.

[29] We also considered the analogous sigma expansions of the ZSM-12 model proposed by LaPierre et al. (R. B. LaPierre, A. C. Rohrman, Jr., J. L. Schlenker, J. D. Wood, M. K. Rubin, W. J. Rohrbaugh, *Zeolites* **1995**, *5*, 346–348), but these ultimately were found not to be as satisfactory as the MTW14MR model.

[30] C. J. Howard, *J. Appl. Crystallogr.* **1982**, *15*, 615–620.

[31] Examples include reference [18]; b) J. G. Nery, S. Hwang, M. E. Davis, *Microporous Mesoporous Mater.* **2002**, *52*, 19–28; c) A.

[32] V. J. Frilette, W. O. Haag, R. M. Lago, *J. Catal.* **1981**, *67*, 218–222.

[33] S. I. Zones, T. V. Harris, *Microporous Mesoporous Mater.* **2000**, *31*, 35**–**36.

[34] J. Weitkamp, S. Ernst, R. Kumar, *Appl. Catal.* **1986**, *27*, 207–210.

[35] "Zeolites: Facts, Figures, Future": J. Weitkamp, S. Ernst, C. Y. Chen, *Stud. Surf. Sci. Catal.* **1989**, *49*, 1115–1129.

[36] C. Y. Chen, L. W. Finger, R. C. Medrud, C. L. Kibby, P. A. Crozier, I. Y. Chan, T. V. Harris, L. W. Beck, S. I. Zones, *Chem. Eur. J.* **1998**, *4*, 1312–1323.

[37] a) United States Patent Application, US 2002/0085976A1, **2002** and b) S. Elomari, US Patent Application, US 2002/104780, **2002**.

[38] a) S. Elomari, US Patent 6464956, **2003** and b) S. Elomari, US Patent 6547958, **2003**.

[39] R. W. Grosse-Kunstleve, L. B. McCusker, C. Baerlocher, *J. Appl. Crystallogr.* **1997**, *30*, 985–995.

[40] R. W. Grosse-Kunstleve, Dissertation ETH No. 11422, Zurich, Switzerland, **1996**.

[41] C. Baerlocher, A. Hepp, W. M. Meier, Dissertation ETH DLS-76, Zurich, Switzerland, **1977**.

[42] Cerius² 2.1. Product of MSI and Biosym.

[43] a) A. K. Rappe, C. J. Casewit, K. S. Colwell, W. A. Goddard III, W. M. Skill, *J. Am. Chem. Soc.* **1992**, *114*, 10024–10035; b) "Studies on Zeolites: Molecular Mechanics, Framework Stability and Crystal Growth": E. de Vos Burchart, Ph.D. Thesis, Technische Universiteit Delft, **1992**, Table I, Chapter XII.

[44] J. P. Olivier, *J. Porous Mater.* **1995**, *2*, 9.

[45] J. P. Olivier, *Carbon* **1998**, *36*, 1469–1472.

[46] A. Saito, H. C. Foley, *Microporous Mater.* **1995**, *3*, 531–542.

[47] B. C. Lippens, J. H. D. Boer, *J. Catal.* **1963**, *4*, 319–323.

[48] "Investigation of Hydrocarbon Adsorption on Large and Extra-Large Pore Zeolites": C. Y. Chen, S. I. Zones, *Stud. Surf. Sci. Catal.* **2001**, *135*, 222.

www.chemeurj.org